2018 IEEE/RSJ International Conference on Intelligent Robots and Systems (IROS)
Madrid, Spain, October 1-5, 2018

Soft-obstacle Avoidance for Redundant Manipulators with Recurrent Neural Network

Yangming Li[1,2], and Blake Hannaford[1]

Abstract— **Compressing soft-obstacles secondary to a controlled motion task is common for human beings. While these tasks are nearly trivial for teleoperated robots, they remain a challenging problem in robotic autonomy. Addressing the problem is significant. For example, in Minimally Invasive Surgeries (MISs), safely compressing soft tissues ensures the surgical safety and decreases tissue removal, thus dramatically decreases surgical trauma and operating room time, and leads to improved surgical outcomes.**

In this work, we define the problem of soft-obstacle avoidance and project the safety motion constraints into the task space and the velocity space. We illustrate the significance of addressing this problem in the robotic surgery scenario. We present a Recurrent Neural Networks (RNNs) based solution, which formulates the problem as an inequality constrained optimization problem and solves it in its dual space. The application of the proposed method was demonstrated in the Raven II surgical robot. Experimental results demonstrated that the proposed method is effective in addressing the soft-obstacle avoidance problem.

Index Terms— **Soft Obstacle Avoidance, Autonomous Robotic Surgery, Robot Arm, Recurrent Neural Network**

I. Introduction

Surgical robots improve dexterity, minimize hand tremor, decrease surgical trauma and deliver decreased postoperative pain, recovery time and hospital stay[1], [2], [3]. Because of the complexity of surgeries, existing surgical robots are often locally teleoperated by human surgeons. However, the desire for further improving surgical outcomes drives the research of autonomous robotic surgeries, because comparing with human beings, surgical robots are neither emotional nor fatigue, and can be more efficient and precise[4], [5].

Driven by the need for improving surgical outcomes, research on robotic surgery autonomy has achieved progress and demonstrated promising results on surgical tasks. For example, Kehoe *et al.* proposed a novel model predictive control algorithm and implemented autonomous multilateral debridement on Raven II surgical robots[6]. Sen *et al.* implemented autonomous suturing through designing a novel needle guide and optimizing needle size, trajectory and control parameters with sequential convex programming[7]. Hu et al. studied the path planner for image-guided semi-autonomous brain tumor ablation and verified the method on Raven II robot[5].

These works effectively demonstrated the feasibility and the advantages of autonomous robotic surgeries. However, environmental obstacles were not considered in these works. And in real Minimally Invasive Surgeries (MISs), both rigid and soft-obstacles are ubiquitous. For rigid obstacles (for example, bony structures), existing obstacle avoidance control schemes can be directly applied. For soft obstacles (for example, muscles, blood vessels and nerves), new control schemes that mimic human experts' "gentle pushing" are desired, in order to decrease surgical trauma and operating room time and to improve surgical outcomes.

In surgeries performed by human surgeons or teleoperated surgical robots, making a pathway by pushing soft obstacles aside naturally happens all the time, with or without explicitly measuring force. However, it is not clear how to "gently push" and existing obstacle avoidance algorithms do not address the problem. More discussion on "gentle push" in surgery is in Subsection III-A.

This work models the soft-obstacle avoidance problem as a constrained optimization problem, where the safety motion pattern constraints are converted into inequality constraints. Thus the soft-obstacle avoidance problem becomes constrained optimization. Recurrent Neural Networks (RNNs) are chosen to solve the problem because of the robustness and the efficiency shared by RNNs based control schemes[8], [9], [10], [11], [12], [13], [14]. In summary, the main contributions of this work are:

- We define the common task of "compressing soft-obstacles secondary to a controlled motion task as the soft-obstacle avoidance problem and illustrate the benefits of addressing the problem in autonomous robotic surgeries.
- We propose a RNN based solution to address the soft-obstacle avoidance problem, while converting the motion pattern constraints into the inequality boundary conditions of RNNs.
- We demonstrate the concept of the proposed method on the Raven II surgical robots in the context of autonomous robotic surgeries. The effectiveness of the proposed method compared with three other control schemes on control precision, robustness against noise and the ability of soft-obstacle avoidance.

II. Redundant Manipulator Rigid Obstacle Avoidance

A. Manipulator Kinematic Control

The manipulator kinematic model defines the nonlinear mapping from the end effector pose (in the task space) to the joint states (in the configuration space), as $\boldsymbol{r}(t) = f\big(\boldsymbol{q}(t)\big)$,

[1]BioRobotics Lab, Department of Electrical Engineering, University of Washington, Seattle, WA, USA 98195
[2]College of Engineering Technology, Rochester Institute of Technology, Rochester, NY, USA 14623

where $\boldsymbol{q}(t) \in \mathbb{R}^{\mathrm{n}}$ is the joint state vector and $\boldsymbol{r}(t) \in \mathbb{R}^{\mathrm{m}}$ is the end effector pose vector, $f(\cdot)$ is the kinematic model[15]. The kinematic control problem is to find the corresponding $\boldsymbol{q}(t)$ for a given $\boldsymbol{r}(t)$, as $\boldsymbol{q}(t) = f^{-1}(\boldsymbol{r}(t))$.

Because the mapping $f(\cdot)$ are often nonlinear and non-convex, it is popular to project the kinematic control problem into the velocity space, through calculating the derivative with respect to time, as: $\dot{\boldsymbol{r}}_{\mathrm{t}} = J\dot{\boldsymbol{q}}_{\mathrm{t}}$, where J is the $n \times m$ Jacobian matrix. Therefore, for full rank non-singular Jacobian matrices, the kinematic control problem can be to simply calculate the inverse Jacobian.

B. Redundant Manipulator Obstacle Avoidance

When the manipulator has more control Degrees of Freedom (DoF) than the task constraint DoF ($n > m$), the manipulator is considered to have kinematic redundancy, and there exists an infinite number of points in its configuration space corresponding to a single point in the task space. This property is widely utilized to address the obstacle avoidance problem, and many intelligent robots are equipped with redundant manipulators for great versatility and broad applicability.

It is natural to treat the obstacle avoidance as an extra constraint and augment the task space with it. This technique has been named Task Space Augmentation, and a family of these algorithms have been extensively studied and successfully applied in real world applications[15], [16]. Mathematically, this technique is described as:

$$\begin{aligned} \dot{\boldsymbol{r}}_{\mathrm{At}} &= J_{\mathrm{A}}\dot{\boldsymbol{q}}_{\mathrm{t}} \\ J_{\mathrm{A}} &= [J^{\mathrm{T}}, J_{\mathrm{o}}^{\mathrm{T}}]^{\mathrm{T}} \\ \boldsymbol{r}_{\mathrm{A}}(t) &= [f\big(\boldsymbol{q}(t)\big)^{\mathrm{T}}, f_o\big(\boldsymbol{q}(t)\big)^{\mathrm{T}}]^{\mathrm{T}} \end{aligned} \tag{1}$$

, where $f_{\mathrm{o}}(\boldsymbol{q}(t)) \in \mathbb{R}^{\mathrm{p}}$ corresponds to the obstacle avoidance constraint and p is the dimension of the constraint.

Another family of classical solutions converts the obstacle avoidance constraint into a cost function $h(\boldsymbol{q})$ and the joint velocity vector, $\dot{\boldsymbol{q}}_0$ that corresponds to obstacle avoidance is determined by the gradient of the cost function[15], [17]. The components of $\dot{\boldsymbol{q}}_0$ located in the null space of J can be selected by $(I - J^{\dagger}J)$, and by adding the selected components to the motion of moving end-effector($J^{\dagger}\dot{\boldsymbol{r}}$), the optimal joint velocity that minimizes $h(\boldsymbol{q})$ will be achieved as: $\dot{\boldsymbol{q}} = J^{\dagger}\dot{\boldsymbol{r}} + (I - J^{\dagger}J)\dot{\boldsymbol{q}}_0$, where $J^{\dagger}$ is the Moore-Penrose pseudo-inverse defined as $J^{\dagger} = J^{\mathrm{T}}(JJ^{\mathrm{T}})^{-1}$.

III. Recurrent Neural Networks for Soft-obstacle Avoidance

A. Soft-obstacle Avoidance in Robotic Surgery

The importance of the soft-obstacle avoidance problem in surgeries was identified when we were studying the correlations between motion patterns and the surgical skill levels in endoscopic skull base surgeries[18], [19], [20]. It is well known that experienced surgeons generate less bone and soft tissue removal than novice surgeons, which not only decreases surgical trauma and recovery time, but also leads to lower health care costs and reduces the possibility of infection[21]. When we watched experienced surgeons performing sinus and skull base operations, we found they have better dexterity which allows compression of soft tissues(Fig.1). It is straightforward to show that soft-obstacle avoidance leads to decreased surgical removal, because allowing soft tissue compression enlarges the configuration space, which enlarges the task space.

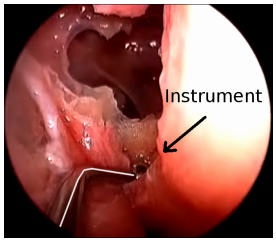

Fig. 1: Endoscopic View of Minimally Invasive Skull Base Surgery on a Cadaver. An expert surgeon was inserting an instrument and an endoscope through the left and the right nostrils, respectively, to reach the pathology. The experiment demonstrated that gently pushing soft tissues effectively decreases the surgical trauma and the operating room time.

Inspired by observing human expert surgeons' operations, the problem of "soft-obstacle avoidance" in robotic surgeries is defined as: *the contact between the manipulator links and soft obstacles is allowed, under the condition that the deformation of a soft obstacle does not lead to damage, such as tearing*. Soft-obstacle avoidance is ubiquitous in Minimally Invasive Surgeries (MISs), thus is critical in automated robotic surgeries, however, remains a challenge.

From the robotics perspective, the soft-obstacle avoidance problem *is different from the compliance control problem and the constrained motion control problem* in the context of robotic surgeries. The latter two were often used in end effector motion optimization for improving surgical outcomes in teleoperated robotic surgeries. For example, cutting tissues requires the control of both the position and the force of the end effector[22], [23], and compliance control is suitable for these tasks. Suturing requires the end effector to move with desired velocities, and constrained motion control can address the problem[24]. The soft-obstacle avoidance requires that all links of a manipulator should not compress soft tissues deeper or faster than the safety thresholds. While it is easy to check with these rules for non-redundant manipulators: projecting the desired end effector position and velocity to the contact points and comparing with the thresholds[25], for redundant manipulators, the redundancy can be and should be used to minimize the safety risk. RNN control schemes are competent to these requirements, as discussed in Section III-C.

B. RNN Control Scheme with Improved Control Precision

The constrained optimization of redundant manipulator motions can be modeled as a Quadratic Programming problem: the defined cost function is the optimization target and the optimization is subject to constraints, such as the kinematic model, the joint limits etc.[13]. The process can

be mathematically defined as:

$$\min_{\dot{q}} \ \dot{q}^{\mathrm{T}} W \dot{q} + c^{\mathrm{T}} \dot{q} \tag{2a}$$

$$\text{s.t. } \dot{r}_{\mathrm{d}} = J\dot{q}, \tag{2b}$$

$$q \in \Omega \tag{2c}$$

where $J = \partial f / \partial q \in \mathbb{R}^{\mathrm{m}\times\mathrm{n}}$, $\dot{r}_{\mathrm{d}} = \partial r(t)/\partial t \in \mathbb{R}^{\mathrm{m}}$, and $\dot{q} = \partial q/\partial t$, and $\Omega \subset \mathbb{R}^{\mathrm{n}}$ denotes the set of the valid joint angles.

The problem can be more efficiently solved in its dual space, through introducing the Lagrange multiplier and projecting the problem into its dual space[13]:

$$L(u,\lambda) = u^{\mathrm{T}} u + \lambda^{\mathrm{T}}(\dot{r}_{\mathrm{d}} - Ju), \tag{3}$$

where u is the dual vector of $\dot{q}$[13], [26].

Though the introduction of Eqn.3, it can be proved that through the Karush-Kuhn-Tucker condition, the solution to Eqn.2 equals the solution to the following equation[27], [28]:

$$\begin{aligned} u &= P_{\Omega}(u - \frac{\partial L}{\partial u}) \\ \dot{r}_{\mathrm{d}} &= Ju \end{aligned} \tag{4}$$

, where P_{Ω} is a projection function that reflects the boundary conditions[13], [26].

Eqn. 4 reminds us of Recurrent Neural Networks as it is the equation of the neural dynamics of a projected RNN (Eqn. 5). More importantly, it has been proven that the equilibrium of the projected RNN equals the optimal solution of the original problem (Eqn.2)[13], [29], [26].

$$\varepsilon \dot{u} = -u + P_{\Omega}(u - \frac{\partial L}{\partial u}), \tag{5a}$$

$$\varepsilon \dot{\lambda} = \dot{r}_{\mathrm{d}} - Ju \tag{5b}$$

where $\varepsilon > 0$ is a scaling factor. $P_{\Omega}(x) = \mathrm{argmin}_{y\in\Omega}||y-x||$ is a projection function from domain Ω' to Ω, where $x \in \Omega'$ and $y \in \Omega$.

However, the control scheme described in Eqn. 5 is subject to error accumulation[8]. In order to improve control precision, we close the loop of position tracking by feeding the position tracking error, $e = r_{\mathrm{d}} - r$, back into the optimization target function, where r_{d} is the desired target and r is the true position from observations and/or estimations. Therefore, the control scheme evolves to[8]:

$$\begin{aligned} u &= P_{\Omega}(-kJ^{\mathrm{T}}(r - r_{\mathrm{d}})). \\ \dot{r}_{\mathrm{d}} &= Ju \end{aligned} \tag{6}$$

The projection function P_{Ω} bounds the neural activities. In order to fulfill the joint limits, we need to project the limits from the joint angle space to the joint velocity space as[8]:

$$P_{\Omega}(x) = \begin{cases} d^- & \text{for} \quad x \le d^- \\ x & \text{for} \quad d^- < x < d^+ \\ d^+ & \text{for} \quad d^+ \le x \end{cases} \tag{7}$$

, with boundary conditions as:

$$\begin{cases} d^- &= c_1(q - q^-) \\ d^+ &= c_2(q^+ - q), \end{cases} \tag{8}$$

where q denotes the joint angle, q^+ and q^- are the upper and the lower joint limits; and c_1 and c_2 are two positive scaling factors. Intuitively, while the joint is approaching its limits, its corresponding boundary condition approaches to zero, thus the robot arm will not break the joint limits. The two scaling factors can adjust the absolute magnitude of joint velocities and the smoothness of velocity decrease.

C. Inequality Constraints Optimization for Soft-obstacle Avoidance

There are many strategies for the rigid obstacle avoidance problem. For example, an efficient way for redundant manipulators is to construct constraints for avoiding the collision and augment the task space with it (Eqn.1)[30]. Generally, the collision can be avoided by forcing the potential collision links to stop or to move toward the "escaping" direction. This can be mathematically explained as:

$$\dot{r}_{\mathrm{o}} = J_{\mathrm{o}}\dot{q}, \tag{9}$$

where $\dot{r}_{\mathrm{o}}$ is the velocity at the potential collision point on the robot arm, J_{o} is the Jacobian with respect to this point, and $\dot{q}$ is the joint velocity. So making $\dot{r}_{\mathrm{o}}$ to stay at zero, or to be a velocity that points to the escaping direction can avoid the collision.

However, two mainly disadvantages prevent applying the scheme (described in Eqn.9) to the soft-obstacle avoidance problem. One is, the contact is not preferable but is still allowed, if the contact is conducted in a "safe manner". Secondly, augmenting task space adds extra constraints which "consume" redundancy, while the redundancy is valuable for the motion optimization.

In order to address these problems, the proposed method converts the soft-obstacle avoidance problem to inequity boundary conditions, so contact is allowed, but also safe motion patterns are enforced by the RNN neural activity boundary conditions and do not consume the robot arm redundancy.

$$\dot{r}_{\mathrm{o}} > J_{\mathrm{o}}\dot{q}, \tag{10}$$

where $\dot{r}_{\mathrm{o}} = \mathrm{sign}\big(k(r_{\mathrm{o}})\big) \circ v_{\max}(d_{\mathrm{c}})$ is *the safe velocity threshold*, operator $\circ$ indicates Hadamard product (element-wise product), function $\mathrm{sign}(x)$ is the sign function (-1, 0, and 1 for $x < 0$, $x = 0$ and $x > 0$, respectively), $k(r_{\mathrm{o}})$ is the direction of velocities, which points to the counter-direction of the compression as: $r_{\mathrm{o},0} - r_{\mathrm{o}}$, where $r_{\mathrm{o},0}$ is the initial tissue contacting position. $v_{\max}(d_{\mathrm{c}})$ is *the maximum allowed speed for safe contact*, which correlates to the compression depth $d_{\mathrm{c}} = ||r_{\mathrm{o},0} - r_{\mathrm{o}}||$ of soft tissues.

With the inequity defined in Eqn. 10, the RNN control scheme can find the optimal (defined by the optimization target function in Eqn. 2) joint velocities that fulfill all constraints (joint limits, contact motion etc.). However, the maximum allowed compression depth d_{cMax} is not fulfilled by the scheme yet. In order to do so, the requirement to exert no more compression than d_{cMax} can be achieved by forcing the $v_{\max}(d_{\mathrm{cMax}}) = 0$. Similarly, the corresponding joint velocity will be $\dot{q}_{\mathrm{oMax}}$. Therefore, the soft-obstacle avoidance

can be achieved by modifying the boundary conditions to the following form, as:

$$\begin{cases} d_{\mathrm{i}}^{-} &= \max\left(c_1(\boldsymbol{q}_{\mathrm{i}}-\boldsymbol{q}_{\mathrm{i}}^{-}),\dot{q}_{\mathrm{s,i}}\right) \\ d_{\mathrm{i}}^{+} &= c_2(\boldsymbol{q}_{\mathrm{i}}^{+}-\boldsymbol{q}_{\mathrm{i}}) \end{cases} \text{, for } \dot{q}_{\mathrm{s,i}} \leq 0$$
$$\begin{cases} d_{\mathrm{i}}^{-} &= c_1(\boldsymbol{q}_{\mathrm{i}}-\boldsymbol{q}_{\mathrm{i}}^{-}) \\ d_{\mathrm{i}}^{+} &= \min\left(c_2(\boldsymbol{q}_{\mathrm{i}}^{+}-\boldsymbol{q}_{\mathrm{i}}),\dot{q}_{\mathrm{s,i}}\right) \end{cases} \text{, otherwise,} \quad (11)$$

where $\dot{q}_{\mathrm{s,i}} = \min(\dot{q}_{\mathrm{o,i}}, \dot{q}_{\mathrm{oMax,i}})$, $i = 1,\cdots,n$ denotes the i-th link.

In summary, the proposed soft-obstacle avoidance control scheme is mathematically described as Enq.6 with the projection function defined in Eqn.7 under the boundary conditions described in Eqn. 11.

IV. Experimental Result and Discussion

RNN control schemes have demonstrated improved computational efficiency, precision and robustness, comparing with their numerical equivalents[9]. In this section, we will compare the proposed method with representative RNN control schemes on the precision, the robustness and the ability of obstacle avoidance.

RNN control schemes have demonstrated improved computational efficiency, precision, and robustness, comparing with their numerical equivalents[9]. In this section, we will compare the proposed method with representative RNN control schemes on the precision, the robustness and the ability of obstacle avoidance.

To our best knowledge, the proposed method is the first RNN control scheme that is capable of soft-obstacle avoidance. To provide a benchmark, three popular RNN control schemes were compared with the proposed method.For quick reference, these algorithms are referred as "Method1", "Method2" and "Method3". "Method1" [30] addresses the obstacle avoidance problem for redundant manipulators in the velocity space. "Method2" [31] addresses the obstacle avoidance problem in the acceleration space. "Method3" [32] optimizes motion in obstacle-free environments, but it addresses the error accumulation problem.

The four algorithms were compared in software simulation for the Raven II surgical robot, a popular surgical robot platform that has been deployed at 17 sites world wide[33]. The mechanical design, the kinematic model and the dynamic model, and the parameters of simulation can be found in [34]. $k = 100$, $c_1 = c_2 = 0.5$ were chosen empirically for the proposed method.

A. Control Precision

The control precision was verified in simulation experiments. The task is to pursue a circular trajectory and the 7-th DoF of Raven is not utilized, so *the task DoF is three and the manipulator DoF is six*. Because "Method3" has superior precision, but is not capable of obstacle avoidance, all four algorithms were compared in obstacle free environments. Method1 and Method2 suffer from error accumulations, so the manipulator starts on the trajectory; the other two methods have random start positions. An example trajectory from the proposed method was shown in Fig.2, from which we can see that even though the arm has huge initial tracking error, its errors converge quickly and follows the desired trajectory. The tracking errors of the four algorithms were shown in Fig.3 and listed in Table I. From these results, it is clear that the proposed method has an advantage on the control precision.

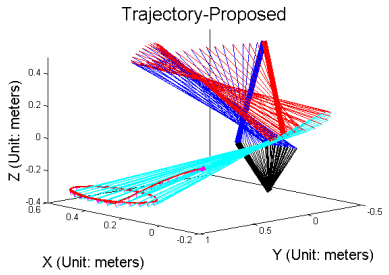

Fig. 2: Tracking a Circular Trajectory with Proposed Method in Obstacle Free Environment. Raven II started from a random position, and the initial arm pose is indicated by thick colored lines. The links' trajectories were indicated by thin colored lines. The desired trajectory was indicated by green lines, which is overlaps by the end effector trajectory indicated by red lines. It is clear that because the proposed method does not suffer from the error accumulation, even though the initial tracking error is big, the errors converge fast.

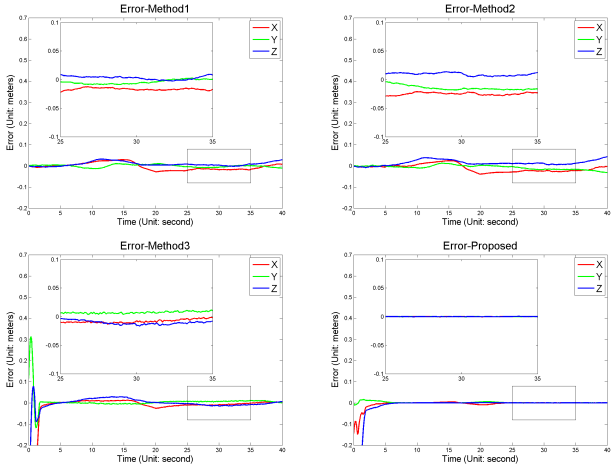

Fig. 3: Tracking Error Comparison of the Four Algorithms on Circular Trajectory Tracking.

TABLE I: RMS Position Tracking Error Comparison.

	Method1[30]	Method2[31]	Method3[32]	Proposed
RMS	0.0280	0.0249	0.0089	0.0081

B. Robustness Against Noise

Because of the cable driven mechanism, surgical robots model uncertainties reduce control precision[35]. The proposed method closed the control loop with a feedback of control errors to improve robustness to process noise. In order to verify the robustness against additive process noise, we artificially injected Gaussian White noise with standard

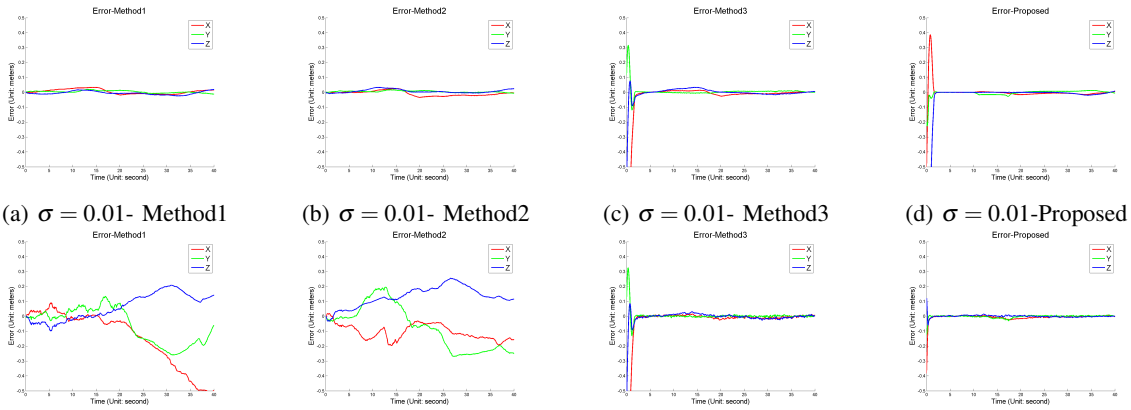

(a) $\sigma = 0.01$- Method1 (b) $\sigma = 0.01$- Method2 (c) $\sigma = 0.01$- Method3 (d) $\sigma = 0.01$-Proposed

(e) $\sigma = 0.25$- Method1 (f) $\sigma = 0.25$- Method2 (g) $\sigma = 0.25$- Method3 (h) $\sigma = 0.25$-Proposed

Fig. 4: Tracking Robustness Against Additive Gaussian White Noise.

deviations: $\sigma = 0.01$ and $\sigma = 0.25$. We are aware that probably no manipulator has control error as bad as $\sigma = 0.25$ (about 43° for revolute joints and 0.75m for prismatic joints with 99.7% confidence), but the extremity is helpful for the verification purpose.

Fig.4 shows the tracking errors with respect to noise levels. From the figures we can see that both Method3 and the proposed method have better robustness by avoiding error accumulations.

C. Obstacle Avoidance

As Method3 is not capable of obstacle avoidance, thus was excluded from the obstacle avoidance experiments.

In the experiments, we use a plane-shaped obstacle and located the target behind the plane to simulate the scenario that a surgical robot is required to reach a target beyond a surgical pathway boundary. In order to better visualize experimental results, we purposely increased the maximum allowed compression depth $d_{\text{cMax}} = 10$cm, for matching the size of Raven II robot. We defined a motion pattern that the allowed velocity to exponentially decrease with respect to compression depth, d_{c}, as: $v_{\text{max}} = -(d_{\text{cMax}}/log(d_{\text{cMax}} - d_{\text{c}}))$. The proposed method can be applied to various definitions of d_{cMax} and v_{max}, according to surgical procedures and tissue types.

Fig.5 visualizes the trajectories of the three methods in soft obstacle. From the figure we can see that while Method1 and Method2 stopped when they reached the boundary, the proposed method compressed the boundary and eventually reached the target. The velocity at the contact points were shown in Fig.6. We can see that Method1 and Method2 were still trying to reach the target but the velocities at the contact points remained nearly zero, and the proposed method dramatically reduced the velocity at the contract point in order to avoid the damage to the surgical pathway boundary but slowly reached the target, as desired.

The distances between the target and the end effector were compared in Fig.7 to verify that the surgical robot reached the desired target under the proposed control scheme. The clinical significance of the proposed scheme is clear as: an extra cut was avoided by the proposed scheme, thus the surgical trauma and costs can be further decreased in automated robotic surgeries.

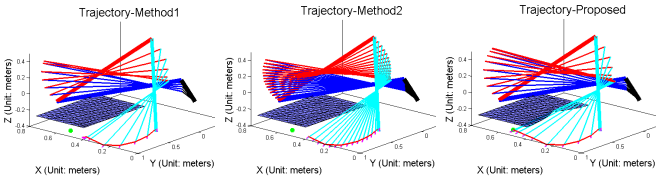

Fig. 5: Trajectory Comparison in Soft-obstacle Avoidance Experiments. The simulated surgical robot was required to reach a target (green ball) behind the soft obstacle (blue plane constituted by triangles). The end effector trajectories were denoted by red lines. The proposed scheme allows the arm to compress the soft obstacle, thus the goal was reached.

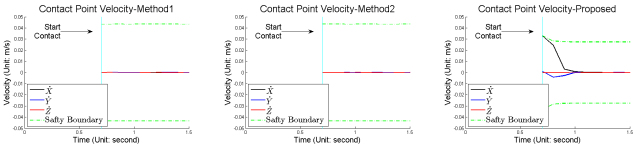

Fig. 6: Contact Point Velocity Comparison. The velocity at *the contact point* was visualized in X, Y and Z directions, respectively. The green dashed line indicates the boundary of damage-free velocities. The proposed scheme regulates the contact velocity and allows the surgical robot to "gently" (the contact velocity and the compression depth are within the defined safety threshold) push a soft obstacle.

V. Conclusion

In this work, a RNN based control scheme was proposed to address the soft-obstacle avoidance problem, which is critical and challenging in autonomous robotic surgeries. The proposed method meets the limits the maximum compression depth and the requirements on motion patterns at the same time thus can be easily applied to various types of soft tissues and surgical procedures. The proposed method can be easily extended to other applications whose constraints can be converted into the compression depth and the velocity patterns.

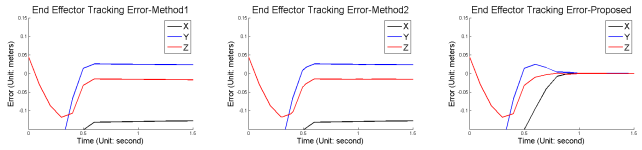

Fig. 7: Distance between Target and End Effector Comparison. The distance between the target and the end effector were compared to verify that the surgical robot reached the desired target under the proposed control scheme.

ACKNOWLEDGMENT

This work was supported by NSF grant IIS-1637444, NIH grant 5R21EB016122-02 and the Korean Institute of Science and Technology (KIST).

REFERENCES

[1] M. J. Mack, "Minimally invasive and robotic surgery," *Jama*, vol. 285, no. 5, pp. 568–572, 2001.

[2] C. Diaz-Arrastia, C. Jurnalov, G. Gomez, and C. Townsend, "Laparoscopic hysterectomy using a computer-enhanced surgical robot," *Surgical endoscopy*, vol. 16, no. 9, pp. 1271–1273, 2002.

[3] J. Clark, D. P. Noonan, V. Vitiello, M. H. Sodergren, J. Shang, C. J. Payne, T. P. Cundy, G.-Z. Yang, and A. Darzi, "A novel flexible hyper-redundant surgical robot: prototype evaluation using a single incision flexible access pelvic application as a clinical exemplar," *Surgical endoscopy*, vol. 29, no. 3, pp. 658–667, 2014.

[4] Y. Li, S. Li, and B. Hannaford, "A novel recurrent neural network control scheme for improving redundant manipulator motion planning completeness," in *Robotics and Automation (ICRA), 2018 IEEE International Conference on*. IEEE, 2018, p. 1 6.

[5] D. Hu, Y. Gong, B. Hannaford, and E. J. Seibel, "Path planning for semi-automated simulated robotic neurosurgery," in *Intelligent Robots and Systems (IROS), 2015 IEEE/RSJ International Conference on*. IEEE, 2015, pp. 2639–2645.

[6] B. Kehoe, G. Kahn, J. Mahler, J. Kim, A. Lee, A. Lee, K. Nakagawa, S. Patil, W. D. Boyd, P. Abbeel, and K. Goldberg, "Autonomous multilateral debridement with the raven surgical robot," in *Robotics and Automation (ICRA), 2014 IEEE International Conference on*. IEEE, 2014, pp. 1432–1439.

[7] S. Sen, A. Garg, D. V. Gealy, S. McKinley, Y. Jen, and K. Goldberg, "Automating multi-throw multilateral surgical suturing with a mechanical needle guide and sequential convex optimization," in *Robotics and Automation (ICRA), 2016 IEEE International Conference on*. IEEE, 2016, pp. 4178–4185.

[8] Y. Li, S. Li, M. Miyasaka, A. Lewis, and B. Hannaford, "Improving control precision and motion adaptiveness for surgical robot with recurrent neural network," in *Intelligent Robots and Systems (IROS), 2017 IEEE/RSJ International Conference on*. IEEE, 2017, pp. 1–6.

[9] Z. Zhang, L. Zheng, J. Yu, Y. Li, and Z. Yu, "Three recurrent neural networks and three numerical methods for solving repetitive motion planning scheme of redundant robot manipulators," *IEEE/ASME Transactions on Mechatronics*, 2017.

[10] Y. Li, S. Li, and B. Hannaford, "A model based recurrent neural network with randomness for efficient control with applications," *IEEE Transactions on Industrial Informatics*, pp. 1–10, 2018.

[11] Y. Zhang, J. Wang, and Y. Xia, "A dual neural network for redundancy resolution of kinematically redundant manipulators subject to joint limits and joint velocity limits," *IEEE transactions on neural networks*, vol. 14, no. 3, pp. 658–667, 2003.

[12] L. Jin, S. Li, X. Luo, and Y. Li, "Neural dynamics for cooperative control of redundant robot manipulators," *IEEE Transactions on Industrial Informatics*, pp. 1–10, 2018.

[13] Y. Xia and J. Wang, "A dual neural network for kinematic control of redundant robot manipulators," *IEEE Transactions on Systems, Man, and Cybernetics, Part B (Cybernetics)*, vol. 31, no. 1, pp. 147–154, 2001.

[14] S. Li, J. He, Y. Li, and M. U. Rafique, "Distributed recurrent neural networks for cooperative control of manipulators: A game-theoretic perspective," *IEEE transactions on neural networks and learning systems*, vol. 28, no. 2, pp. 415–426, 2017.

[15] B. Siciliano, "Kinematic control of redundant robot manipulators: A tutorial," *Journal of Intelligent & Robotic Systems*, vol. 3, no. 3, pp. 201–212, 1990.

[16] A. M. Zanchettin and P. Rocco, "A general user-oriented framework for holonomic redundancy resolution in robotic manipulators using task augmentation," *IEEE Transactions on Robotics*, vol. 28, no. 2, pp. 514–521, 2012.

[17] D. Nguyen-Tuong and J. Peters, "Model learning for robot control: a survey," *Cognitive processing*, vol. 12, no. 4, pp. 319–340, 2011.

[18] R. A. Harbison, Y. Li, A. M. Berens, R. A. Bly, B. Hannaford, and K. S. Moe, "An automated methodology for assessing anatomy-specific instrument motion during endoscopic endonasal skull base surgery," *Journal of Neurological Surgery Part B: Skull Base*, vol. 38, no. 03, pp. 222–226, 2017.

[19] Y. Li, R. A. Bly, R. A. Harbison, I. M. Humphreys, M. E. Whipple, B. Hannaford, and K. S. Moe, "Anatomical region segmentation for objective surgical skill assessment with operating room motion data," *Journal of Neurological Surgery Part B: Skull Base*, vol. 369, no. 15, pp. 1434–1442, 2017.

[20] R. A. Harbison, A. M. Berens, Y. Li, R. A. Bly, B. Hannaford, and K. S. Moe, "Region-specific objective signatures of endoscopic surgical instrument motion: A cadaveric exploratory analysis," *Journal of Neurological Surgery Part B: Skull Base*, vol. 78, no. 01, pp. 099–104, 2017.

[21] P. Van Hove, G. Tuijthof, E. Verdaasdonk, L. Stassen, and J. Dankelman, "Objective assessment of technical surgical skills," *British Journal of Surgery*, vol. 97, no. 7, pp. 972–987, 2010.

[22] R. H. Taylor, A. Menciassi, G. Fichtinger, P. Fiorini, and P. Dario, "Medical robotics and computer-integrated surgery," in *Springer handbook of robotics*. Springer, 2016, pp. 1657–1684.

[23] Y. Li and B. Hannaford, "Gaussian process regression for sensorless grip force estimation of cable-driven elongated surgical instruments," *IEEE Robotics and Automation Letters*, vol. 2, no. 3, pp. 1312–1319, 2017.

[24] A. Kapoor, N. Simaan, and R. H. Taylor, "Suturing in confined spaces: Constrained motion control of a hybrid 8-dof robot," in *Advanced Robotics, 2005. ICAR'05. Proceedings., 12th International Conference on*. IEEE, 2005, pp. 452–459.

[25] T. Yoshikawa, *Foundations of robotics: analysis and control*. MIT press, 1990.

[26] Y. Zhang, J. Wang, and Y. Xu, "A dual neural network for bi-criteria kinematic control of redundant manipulators," *IEEE Transactions on Robotics and Automation*, vol. 18, no. 6, pp. 923–931, 2002.

[27] S. Boyd and L. Vandenberghe, *Convex optimization*. Cambridge university press, 2004.

[28] S. Li, S. Chen, B. Liu, Y. Li, and Y. Liang, "Decentralized kinematic control of a class of collaborative redundant manipulators via recurrent neural networks," *Neurocomputing*, 2012.

[29] Y. Li, J. Zhang, and S. Li, "STMVO: biologically inspired monocular visual odometry," *Neural Computing and Applications*, vol. 29, no. 6, pp. 215–225, 2018.

[30] Y. Zhang and J. Wang, "Obstacle avoidance for kinematically redundant manipulators using a dual neural network," *IEEE Transactions on Systems, Man, and Cybernetics, Part B (Cybernetics)*, vol. 34, no. 1, pp. 752–759, 2004.

[31] D. Guo and Y. Zhang, "Acceleration-level inequality-based man scheme for obstacle avoidance of redundant robot manipulators," *IEEE Transactions on Industrial Electronics*, vol. 61, no. 12, pp. 6903–6914, 2014.

[32] S. Li, Y. Zhang, and L. Jin, "Kinematic control of redundant manipulators using neural networks," *IEEE Transactions on Neural Networks and Learning Systems*, 2016.

[33] B. Hannaford, J. Rosen, D. W. Friedman, H. King, P. Roan, L. Cheng, D. Glozman, J. Ma, S. N. Kosari, and L. White, "Raven-II: an open platform for surgical robotics research," *Biomedical Engineering, IEEE Transactions on*, vol. 60, no. 4, pp. 954–959, 2013.

[34] Y. Li, M. Miyasaka, M. Haghighipanah, L. Cheng, and B. Hannaford, "Dynamic modeling of cable driven elongated surgical instruments for sensorless grip force estimation," in *Robotics and Automation (ICRA), 2016 IEEE International Conference on*. IEEE, 2016, pp. 4128–4134.

[35] M. Miyasaka, M. Haghighipanah, Y. Li, and B. Hannaford, "Hysteresis model of longitudinally loaded cable for cable driven robots and identification of the parameters," in *Robotics and Automation (ICRA), 2016 IEEE International Conference on*. IEEE, 2016, pp. 4051–4057.